Establishment and Analysis of Standardized Model of Porpoise External Morphology Based on Computer Vision

Hongbo Cao, Haixu Xi

Abstract—**Morphological analysis was a key step in the study of the diversity of fishery resources. To improve the intelligence and automation of the morphological analysis of Marine organisms, and to reduce the error of the design of the external morphological design of the soft-body bionic porpoise, the standardized model of the external morphological model of porpoises was established and analyzed by using computer vision technology. Firstly, relevant image preprocessing was carried out on the visually sampled porpoise image, and Canny algorithm was used to extract the edge contour of the porpoise body. Then, the coordinates of significant feature points on the porpoise contour were obtained by traversal calculation method. The six mathematical models including Exponential, Fourier, Gaussian, Polynomial, Power function and Sine function were used to fit the outline of the porpoise body. Statistical parameters were used to evaluate the degree to which each model fitted the porpoise body contour. The optimal fitting results were finally selected for optimization analysis with the NACA (National Advisory Committee for Aviation) airfoil. The experimental results showed that the standardization model and the biological morphology analysis were convenient based on computer vision technology. The Polynomial model had the highest degree of comprehensiveness. It was most conducive to the optimization of NACA airfoil shape. This study offered novel insights into porpoise morphological analysis and establishes rich investigative methodologies, while also providing a reference framework for subsequent design of soft bionic porpoises.**

Index Terms—**Computer vision, mathematical model, morphological analysis, NACA airfoil, porpoise**

I. Introduction

PORPOISE belongs to the phylum Chordata, class Mammalia, order Cetacea, family Phocoenidae, and genus Phocoena [1]. It exhibits a compact body size, resembling the smaller, rostrum-less species within the Delphinidae family [2], [3]. The harbor porpoise typically reaches a body length of 1.4 meters and a weight of 42 kilograms, with a maximum recorded length of 1.85 meters, highlighting a marked contrast in body size relative to other common dolphin species within the Delphinidae family [4].

Manuscript received December 6, 2024; revised August 25, 2025.

This work was supported by the 7th "333 High-Level Talent Training Project" of Jiangsu Province under Grant No. (2024) 3-0456.

Hongbo Cao is a lecturer at School of Computer Engineering, Jiangsu University of Technology, Changzhou 213001, China (e-mail: hbcao@jsut.edu.cn).

Haixu Xi is an Associate Professor at School of Computer Engineering, Jiangsu University of Technology, Changzhou 213001, China (corresponding author to provide phone: 008613776826323; e-mail: xihaixu@jsut.edu.cn).

Despite being cetaceans, their smaller size makes them prey to many larger marine animals. Due to their limited numbers and declining population each year, they hold a high conservation status worldwide. Effective conservation of these porpoises, aimed at enhancing marine biodiversity, necessitates morphological analysis and the development of soft bionic underwater vehicles to ensure ecological compatibility with marine fish [5], [6]. In addition, the identification of porpoises or other small marine predators sharing analogous biological traits provided critical ecological insights for marine environment assessment [7].

Since the dawn of the 21st century, the rapid advancement of computer technology in the information age has led to the widespread adoption of computer vision across diverse industries. Notably, computer vision technology had achieved substantial progress in natural resource assessment, precision agriculture, biology, safety monitoring and classification [8], [9], [10]. Researchers such as Maxime Vidal from Switzerland and D.J. White from the UK had applied computer vision-based edge detection techniques to fish image processing, leveraging fin shape characteristics for individual identification and demonstrating significant improvements in efficiency and measurement accuracy relative to manual method [11], [12]. In China, Yu Xinjie and colleagues used computer vision technology to preprocess images of large yellow croaker, accurately obtaining its external morphological parameters [13]. Huang Xiaoshuang and colleagues applied computational biometrics to fit curves to squid body structures and conduct quantitative morphological analysis for the design of bionic squid inspired drag-reduction models. However, the design process relied solely on 3D software-based model construction without a comparative evaluation of the advantages and disadvantages of various mathematical modeling approaches, thereby failing to identify the optimal model for squid curve shape representation [14]. Domestically and internationally, most research on fish identification and bionic design in biology focused on easily captured fish species [15]. However, research on applying computer vision technology to cetaceans within underwater engineering contexts and the comparative evaluation of mathematical models for curve-shape representation remained limited.

In this study, computer vision technology was used to study the curvilinear morphology of porpoise images. By preprocessing sampled data using digital image algorithm (Canny), the curve shapes of the contour of the porpoise body in both the front view and the top view were extracted.

The performance of fitting various mathematical models to these contours was assessed using three evaluation metrics: Sum of Squared Errors (SSE), Root Mean Square Error (RMSE), and Coefficient of Determination (R^2). The best model was selected to establish characteristic mathematical recognition models. To align the resulting mathematical model equations with NACA airfoil equations, the relevant terms were adjusted and recomputed to facilitate optimization. A regression analysis was performed between the optimized mathematical models and NACA airfoil models to identify the NACA airfoil that best matches the porpoise body's front and top contour views. This not only facilitated the application of synergistic soft-bionic biological design but also enhanced understanding of the marine environment and fish's activity ranges, while providing practical theoretical foundations for AI-driven exploration of ecological and bionic mechanisms.

II. Materials and Methods

A. Source of Experimental Data

The primary subject of this study was the harbor porpoise (Phocaena phocaena). To model its body contour, key biological morphological features must be extracted. The species' natural agility in wild environments complicates live capture, and its status as an endangered species underscores the necessity of non-invasive modeling approaches [16]. Therefore, static images from relevant studies [17] were used for processing in Fig. 1.

(a) Front view

(b) Top view

Fig. 1. Front and top views of the Phocaena phocaena

B. Extraction of Contours and Feature Points

The contour extraction of the harbor porpoise was implemented using the Canny algorithm [18], [19], [20], [21], [22], [23]. The traditional Canny algorithm comprises five stages: Gaussian filtering for noise reduction, gradient calculation, non-maximum suppression, double threshold detection, and edge linking. Building upon this foundation, Contrast Limited Adaptive Histogram Equalization (CLAHE) and an adaptive thresholding technique were integrated to enhance the Canny algorithm's performance. First, the grayscale processing of Fig. 1 was performed, which could effectively remove some obvious irrelevant information. The resulting grayscale image underwent processing through Gaussian filtering and connected component analysis to suppress noise while preserving the integrity of biological morphology. Subsequently, CLAHE was applied to enhance the grayscale image, thereby optimizing edge detection performance under variable lighting conditions. Then, the Sobel operator was applied to compute the image's gradient magnitude and direction, which facilitates non-maximum suppression (NMS) by suppressing those edge-related gradient values to zero. Subsequently, an adaptive thresholding method leveraging gradient percentiles was implemented to enhance the robustness of contour extraction. Following this adjustment, the upper threshold was set to 250 and the lower threshold was set to 200, ensuring optimal contour extraction from images. Finally, morphological post-processing was performed on the derived image contour map. Opening operations were employed to remove noise and eliminate isolated noise points, while closing operations connected fragmented edges to preserve contour continuity, ultimately producing a refined contour edge image (Fig. 2).

In the experiment, distinct curve fitting operations were implemented for the front and top view contours of the porpoise, based on the inherent asymmetry of the front view and the symmetry of the top view. Specifically, for the front view, separate curve fitting procedures were applied to the dorsal contour and the lower body contour (spanning from the anterior tip of the body to the notch preceding the tail fin), with the fitted curves subsequently combined to form a complete contour representation. In contrast, the top view required only a single curve fitting operation on the upper body contour, as its symmetrical structure simplifies the process. To more accurately acquire the characteristic points of the finless porpoise, a feature point extraction approach based on distance transformation (Distance Transform) was implemented, combined with a morphological skeletonization algorithm. This method involved traversing the extracted porpoise contour from the anterior tip of the upper jaw to systematically identify key anatomical feature points. Leveraging previous research findings, we annotated these critical feature points. (Fig. 2 illustrated the process, and detailed data were presented in Table I.) [24], [25].

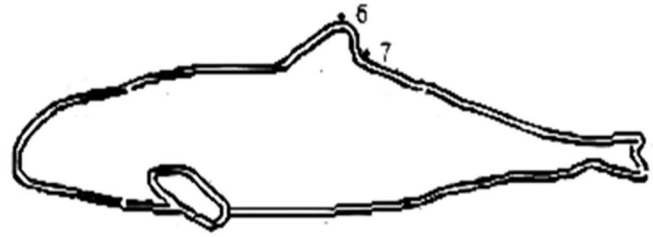

(a) Front view

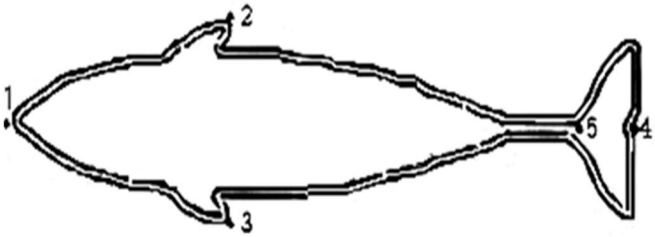

(b) Top view

Fig. 2. The calibration map of edge-detected feature points on the porpoise across different views.

C. Methods for Discovering Curve Morphology

To assess the compatibility of the finless porpoise's front

and top view contours with diverse mathematical curve models, regression analysis was conducted on the contours using the Curve Fitting Toolbox in MATlab software. For each view, the horizontal pixel coordinates of the contour were designated as independent variables, while the vertical pixel coordinates served as dependent variables. Scatterplots (Fig. 3) were generated to facilitate fitting to mathematical curve models.

TABEL I
The description and coordinates of the feature points of porpoise

Feature points	Description	Feature point coordinates	
		X	Y
1	Maxillary anterior end	6.1	1
2	Wing base (upper)	85.4	19.87
3	Wing base (lower)	85.4	-19.87
4	Lacking tail fin	232.3	1.11
5	Basal part of caudal fin	229.6	22.01
6	Dorsal fin tip	122	62.6
7	Dorsal fin posterior base	130.9	32.1

The process sought to develop a multiple regression model characterizing the curvilinear morphology of the harbor porpoise. The optimal mathematical model was selected through a systematic comparison of goodness-of-fit metrics across competing models.

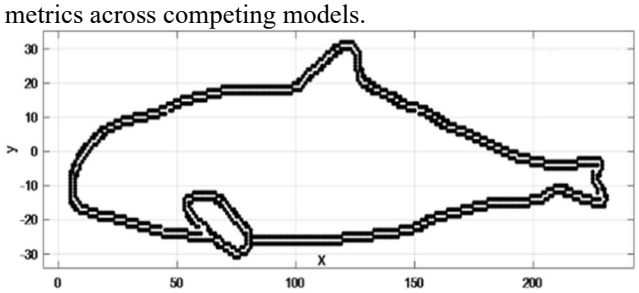

(a) Front view

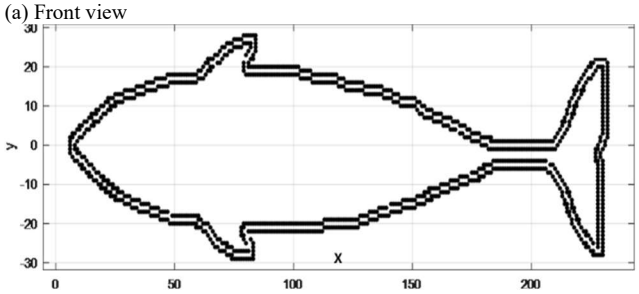

(b) Top view

Fig. 3. Scatterplot of porpoise body in different views

A total of six curve mathematical models were selected for this study, as detailed in Table II, which presented theoretical formulations prior to data input. Fig. 3 displayed the scatterplots of the porpoise body in both front and top view, with the coordinate origin defined at the anterior tip of the upper jaw.

The goodness-of-fit of curve models was typically evaluated by comparing statistical metrics such as SSE, RMSE, and R^2 to assess their relative performance [26], [27].

The calculation formulas for SSE, RMSE, and R^2 were as follows:

$$SSE = \sum_{i=1}^{n} (y_i - \hat{y}_i)^2 \tag{1}$$

$$RMSE = \sqrt{\frac{1}{n}\sum_{i=1}^{n} (y_i - \hat{y}_i)^2} \tag{2}$$

$$R^2 = 1 - \frac{\sum_i^n (y_i - \hat{y}_i)^2}{\sum_i^n (y_i - \overline{y_i})^2} \tag{3}$$

In the context of these formulas, y_i represented the true value, $\hat{y}_i$ represented the predicted value, and $\overline{y_i}$ represented the mean. Lower values of SSE and RMSE typically correlated with improved model fit and enhanced predicative accuracy, while an R^2 value closer to 1 indicated a more precise alignment between the curve and the data.

TABLE II
Curve model formula

Model	Formula
Exponential	$y = ae^{bx} + ce^{dx}$
Fourier	$y = a_0 + \sum_{i=1}^{n} a_i \cos(i\omega x) + b_i \sin(i\omega x)$
Gaussian	$y = \sum_{i=1}^{n} a_i e^{\left[-\left(\frac{x-b_i}{c_i}\right)^2\right]}$
Polynomial	$y = \sum_{i=1}^{n+1} p_i x^{n+1-i}$
Power function	$y = ax^b + c$
Sine	$y = \sum_{i=1}^{n} a_i \sin(b_i x + c_i)$

III. Results and Analysis

A. Analysis of the Porpoise Body Contour Fitting from the Front View

The comparison results of various models for the dorsal and lower body contours of the porpoise in the front view, following curve fitting with different numbers of polynomial terms, were presented in Table III and Table IV.

TABLE III
Fitting results of the dorsal contour by different models

Number of terms or degree	Model	SSE	RMSE	R^2
1	Exponential	1941	9.308	0.142
	Fourier	215.1	3.106	0.897
	Gaussian	270.0	3.472	0.881
	Polynomial	189.1	9.169	0.167
	Power function	226.0	10.02	0.057
	Sine	345.2	3.925	0.848
2	Exponential	250.3	10.59	0.102
	Fourier	167.4	2.752	0.926
	Gaussian	582.0	1.623	0.974
	Polynomial	381.4	4.126	0.832
	Power function	109.5	6.994	0.517
	Sine	318.7	3.772	0.859
3	Fourier	105.6	2.196	0.953
	Gaussian	109.6	2.242	0.951
	Polynomial	200.7	0.949	0.991
	Sine	318.7	3.772	0.859
4	Fourier	901.3	2.037	0.960
	Gaussian	268.4	1.116	0.988
	Polynomial	180.1	0.863	0.993
	Sine	557.3	1.610	0.975
5	Fourier	436.2	1.424	0.980
	Gaussian	188.9	0.944	0.991
	Polynomial	397.3	1.340	0.982
	Sine	200.7	1.013	0.990
6	Fourier	404.5	1.378	0.982
	Gaussian	391.8	1.369	0.982
	Polynomial	227.3	1.016	0.992
	Sine	217.7	1.020	0.990
7	Fourier	215.7	1.011	0.990
	Gaussian	425.2	1.436	0.981
	Polynomial	370.3	1.300	0.983
	Sine	236.0	1.070	0.989
8	Fourier	197.7	0.972	0.991
	Gaussian	105.4	2.279	0.953
	Polynomial	388.1	1.334	0.992
	Sine	213.1	1.024	0.980

The Exponential and Power function models were restricted to quadratic forms. Consequently, at the third order and beyond, only the Fourier, Gaussian, Polynomial, and Sine models were evaluated and compared. Through varying the number of terms or polynomial degree for each model, the fitted curve's morphology and statistical metrics (SSE, RMSE, and R^2) were assessed to identify the optimal fitting equation. The analysis of comparison results revealed that, as the term count or polynomial degree increases, the Fourier, Gaussian, Polynomial, and Sine models demonstrated superior performance in fitting the dorsal contour of the harbor porpoise.

TABLE IV
Fitting results of lower body contours by different models

Number of terms or degree	Model	SSE	RMSE	R^2
1	Exponential	423.1	4.336	0.268
	Fourier	209.9	0.970	0.963
	Gaussian	327.9	1.209	0.943
	Polynomial	395.3	4.191	0.316
	Power function	555.3	4.968	0.039
	Sine	545.4	1.560	0.905
2	Exponential	530.6	4.877	0.082
	Fourier	168.2	0.872	0.970
	Gaussian	190.8	0.929	0.967
	Polynomial	200.4	0.946	0.965
	Power function	200.5	2.992	0.653
	Sine	192.3	0.932	0.966
3	Fourier	128.3	0.765	0.977
	Gaussian	131.4	0.776	0.977
	Polynomial	179.1	0.896	0.969
	Sine	128.2	0.766	0.977
4	Fourier	127.2	0.765	0.978
	Gaussian	121.8	0.752	0.978
	Polynomial	17.76	0.282	0.996
	Sine	114.8	0.730	0.980
5	Fourier	106.0	0.702	0.981
	Gaussian	107.6	0.712	0.981
	Polynomial	20.67	0.305	0.996
	Sine	104.5	0.702	0.981
6	Fourier	88.67	0.645	0.984
	Gaussian	100.9	0.694	0.982
	Polynomial	23.12	0.324	0.996
	Sine	96.49	0.679	0.983
7	Fourier	85.22	0.635	0.985
	Gaussian	95.70	0.681	0.983
	Polynomial	28.28	0.359	0.995
	Sine	88.25	0.654	0.984
8	Fourier	76.03	0.603	0.986
	Gaussian	64.35	0.563	0.988
	Polynomial	33.74	0.393	0.994
	Sine	78.60	0.622	0.986

These models demonstrated their respective advantages under varying levels of complexity. For example, the Fourier model was adept at capturing complex fluctuation characteristics, the Gaussian model was suitable for local smooth fitting, the Polynomial model offered high accuracy in fitting overall trends, and the Sine model was particularly effective at describing periodic features. The formulas were:

$$\begin{aligned} y = {} & 18.72 - 13.63\cos(0.02x) + 9.26\sin(0.02x) \\ & -0.648\cos(0.04x) + 1.579\sin(0.04x) - 3.977\cos(0.06x) \\ & +2.09\sin(0.06x) - 0.684\cos(0.08x) + 0.59\sin(0.08x) \\ & -1.865\cos(0.1x) + 2.832\sin(0.1x) - 0.348\cos(0.12x) \\ & +0.287\sin(0.12x) - 0.125\cos(0.14x) + 1.64\sin(0.14x) \\ & - 0.12\cos(0.16x) + 9.98\sin(0.16x) \end{aligned} \quad (4)$$

$$\begin{aligned} y = {} & 12.92e^{[-(\frac{x-119.1}{11.31})^2]} + 29.28e^{[-(\frac{x-116}{73.56})^2]} + \\ & 4.776e^{[-(\frac{x-221.6}{7.482})^2]} + 11.57e^{[-(\frac{x-51.4}{34.72})^2]} + 7.15e^{[-(\frac{x-21.5}{14.15})^2]} \end{aligned} \quad (5)$$

$$y = 31.53 - 8.852x - 15.62x^2 + 2.507x^3 + 3.025x^4 \quad (6)$$

$$\begin{aligned} y = {} & 35.7\sin(0.01x - 0.135) + 13.62\sin(0.05x - 0.985) \\ & +12.61\sin(0.04x - 1.117) + 3.048\sin(0.11x - 0.148) \\ & +1.53\sin(0.17x - 6.158) \end{aligned} \quad (7)$$

The comparison results in Table III designated Formula (4) as an eight-term Fourier fit, Formula (5) as a five-term Gaussian fit, Formula (6) as a quartic Polynomial fit, and Formula (7) as a five-term Sine fit as the optimal fitting equations for the application. The R^2 values corresponding to these formulas all exceeded 0.90. Therefore, these four models exhibited a good fit for the curvature of the dorsal side of the porpoise body. The comparative analysis of the statistical metrics (SSE and RMSE) across the four models revealed that the Polynomial and Gaussian models exhibit superior fitting accuracy compared to the Fourier and Sine models. The model intended for application in the design or recognition of underwater streamlined soft-bionic vehicles must balance both accuracy requirements and model complexity. In summary, the Polynomial model with n=4, SSE=180.1, RMSE=0.863, and R^2=0.993 could be selected. Therefore, the fitting equation was Formula (6): $y_1 = 31.53 - 8.852x - 15.62x^2 + 2.507x^3 + 3.025x^4$.

The lower body contour of the porpoise was analyzed using the same methodology applied to the dorsal body contour fitting. The following fitting formulas were derived:

$$\begin{aligned} y = {} & 24.04 - 0.32\cos(0.02x) - 0.16\sin(0.02x) \\ & +2.43\cos(0.04x) + 2.03\sin(0.04x) + 1.74\cos(0.06x) \\ & +4.21\sin(0.06x) - 2.63\cos(0.08x) + 1.53\sin(0.08x) \\ & -1.65\cos(0.1x) - 1.05\sin(0.1x) + 0.7\cos(0.12x) \\ & +1.79\sin(0.12x) + 0.59\cos(0.14x) \\ & +0.88\sin(0.14x) + 1.44\cos(0.16x) \\ & +0.23\sin(0.16x) \end{aligned} \quad (8)$$

$$\begin{aligned} y = {} & 28.5e^{[-(\frac{x-12.66}{27.89})^2]} + 19.13e^{[-(\frac{x-43.22}{10.89})^2]} \\ & -73.52e^{[-(\frac{x-178.19}{42.04})^2]} + 9.03e^{[-(\frac{x-159.85}{1.68})^2]} \\ & +37.81e^{[-(\frac{x-178.35}{50.39})^2]} + 10.97e^{[-(\frac{x-279.6}{15.91})^2]} \\ & +29.19e^{[-(\frac{x-2\ .25}{27.8})^2]} + 20.54e^{[-(\frac{x-526.25}{827.8})^2]} \end{aligned} \quad (9)$$

$$y = -24.28 + 5.794x + 6.149x^2 - 1.568x^3 - 0.793x^4 \quad (10)$$

$$\begin{aligned} y = {} & 3.8\sin(0.03x + 1.77) + 30.19\sin(0.05x + 0.34) \\ & +20.67\sin(0.07x - 6.23) + 31.74\sin(0.08x - 0.58) \\ & +26.76\sin(0.11x + 0.34) + 19.19\sin(0.14x - 0.9) \\ & + 11.12\sin(0.15x - 2.39) + 7.82\sin(0.17x + 6.5) \end{aligned} \quad (11)$$

The comparison results in Table IV designated Formula (8) as an eight-term Fourier fit, Formula (9) as an eight-term Gaussian fit, Formula (10) as a quartic Polynomial fit, and Formula (11) as an eight-term Sine fit as the optimal fitting equations for the application. Following the same comparative analysis, the quartic Polynomial model (n=4) with SSE=17.76, RMSE=0.282, and R^2=0.996 were ultimately selected. Therefore, the resulting fitting equation was Formula (10): $y_2 = -24.28 + 5.794x + 6.149x^2 - 1.568x^3 - 0.793x^4$.

From this, it could be inferred that the equation system for fitting the front view contour of the porpoise was:

$$O_1(x) = \begin{cases} 31.53 - 8.852x - 15.62x^2 + 2.507x^3 + 3.025x^4 \\ -24.28 + 5.794x + 6.149x^2 - 1.568x^3 - 0.793x^4 \end{cases} \quad (12)$$

Fig. 4 showed the fitting results of the quartic Polynomial model applied to the dorsal and lower body contours of the porpoise. Since the experiment studied the morphology of harbor porpoises at rest, and the contour lines of the porpoise

body shape were streamlined, while ignoring secondary data on pectoral, dorsal, and caudal fins, it was believed that the body trunk of porpoises follows the NACA airfoil Polynomial of streamlined bodies. Inspired by the NACA airfoil framework, the polynomial-fitted front view contour equations of the porpoise, denoted as $O_1(x)$, were refined by removing constant terms and incorporating half of the independent variable. Consequently, a set of silhouette contour equations for the harbor porpoise in front view, denoted as $C_1(x)$, were derived, aligning with the structure of the NACA airfoil equation system. The equation system was:

$$C_1(x) = \begin{cases} -(7.308e+11)x^{\frac{1}{2}} + (3.65e+11)x - 0.0065x^2 \\ \quad +(1.752e-0.5)x^3 - (0.1966e-0.8)x^4 \\ (9.44e+13)x^{\frac{1}{2}} - (4.72e+13)x - 0.0084x^2 \\ \quad -(6.032e-0.5)x^3 - (1.318e-0.7)x^4 \end{cases} \quad (13)$$

In this study, as the front view contour of the harbor porpoise is asymmetrical, a NACA four-digit asymmetric airfoil was employed to align with its morphological characteristics. A regression analysis was conducted between $C_1(x)$ and various NACA airfoil models. After comparing SSE_1 between $C_1(x)$ and each NACA airfoil model, the results were presented in Table V.

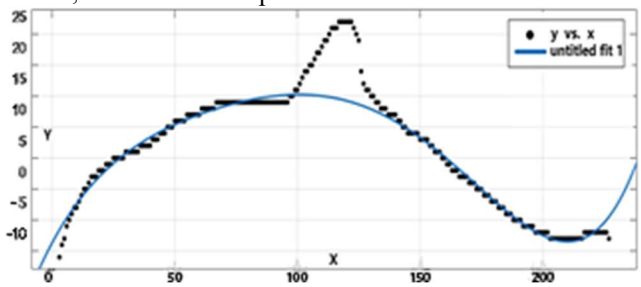

(a) The dorsal body contours

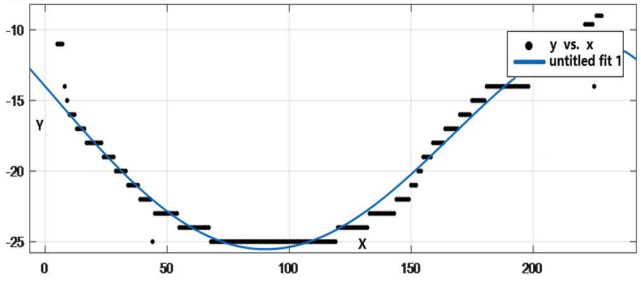

(b) The lower body contours

Fig. 4. Modeling the schematic of the body contours in the front view of the porpoise

According to Table V, the NACA2408 airfoil provided a better fit to the harbor porpoise's body contour. Consequently, it could be selected as the reference contour equation for the front view silhouette of the harbor porpoise in a stationary state. The parameters of the NACA2408 model could be determined by correlating them with the morphological characteristics of the porpoise. By measuring the porpoise's body length (from the tip of the upper jaw to the notch in the tail fluke), the chord length (c) of its hydrodynamic profile could be established. Applying the NACA airfoil theory, this allowed the inference that 2% of c corresponds to the maximum curvature (m), 40% of c defines the curvature peak position (p), and 12% of c represents the maximum thickness (t). Finally, it could be concluded that the front view contour equation of the porpoise was the four-digit asymmetric airfoil NACA2408, and its parameters were: c=226.2, m=4.524, p=90.48, t=18.096.

Table V
The sum of the squared residuals from the regression of NACA airfoil equations and polynomial formulas

NACA airfoil model	SSE_1
2408	215.552608
2410	216.742294
2421	222.557821
2424	225.127964

Note: (SSE_1 represents the sum of squared residuals with the NACA equation and $C_1(x)$)

B. Analysis of the Porpoise Body Contour Fitting from the Top View

The same six models were used for curving the upper body contour in the top view of the porpoise. Considering both accuracy and model complexity, the fitting results for each model were shown in Table VI as the degree or number of terms increases. By analyzing Table VI, the more suitable models for fitting the upper body contour of the porpoise were the Fourier model, Gaussian model, Polynomial model, and Sine model. Their respective formulas were as follows:

$$\begin{aligned} y = {} & -36.43 + 96.04\cos(1.3x) - 14.3\sin(1.3x) \\ & -77.15\cos(2.6x) + 10.5\sin(2.6x) + 59.87\cos(3.9x) \\ & -16.92\sin(3.9x) - 40.66\cos(5.2x) + 19.38\sin(5.2x) \\ & +21.14\cos(6.5x) - 14.9\sin(6.5x) - 8.22\cos(7.8x) \\ & +9.91\sin(7.8x) + 2.705\cos(9.1x) - 3.964\sin(9.1x) \end{aligned} \quad (14)$$

$$\begin{aligned} y = {} & 6.803e^{[-(\frac{x+0.58}{0.04})^2]} + 7.97e^{[-(\frac{x+0.68}{0.09})^2]} \\ & +20.28e^{[-(\frac{x-1.52}{0.13})^2]} + 3.538e^{[-(\frac{x+0.81}{0.08})^2]} - 13.58e^{[-\frac{x+13.41^2}{2.55}]} \\ & +18.44e^{[-(\frac{x+1.02}{1.12})^2]} + 353.4e^{[-(\frac{x-0.04}{0.456})^2]} - 344.7e^{[-(\frac{x-0.04}{0.45})^2]} \end{aligned} \quad (15)$$

$$y = 17.21 - 16x - 9.402x^2 + 7.305x^3 + 2.889x^4 \quad (16)$$

$$\begin{aligned} y = {} & 35\sin(1.4x + 1.7) + 23.73\sin(2.2x - 1.6) \\ & +20.721\sin(4.2x + 1.9) + 20.67\sin(4.2x - 1.19) \\ & +1.332\sin(14.8x - 1.6) + 1.453\sin(9.1x + 0.6) \\ & +1.656\sin(11x - 2.9) + 1.014\sin(16.5x + 1.2) \end{aligned} \quad (17)$$

The comparison results in Table VI designated Formula (14) as a seven-term Fourier fit, Formula (15) as an eight-term Gaussian fit, Formula (16) as a quartic Polynomial fit, and Formula (17) as an eight-term Sine fit as the optimal fitting equations for the application.

Considering the subsequent applications, the Polynomial model at n=4 was ultimately chosen. It had R^2=0.992, SSE=130.0, and RMSE=1.032. The fitting equation was Formula (16): $y_3 = 17.21 - 16x - 9.402x^2 + 7.305x^3 + 2.889x^4$.

Since the porpoise body was symmetrical in the top view, and the consistent method used for similarity value calculation, after comprehensive analysis, the fourth-order polynomial curve model for the lower body contour could be formulated as:

$$y_4 = -17.21 + 16x + 9.402x^2 - 7.305x^3 - 2.889x^4 \quad (18)$$

From this, it could be inferred that the equation system for fitting the contour of the porpoise body in the top view. The equation system was:

$$O_2(x) = \begin{cases} 17.21 - 16x - 9.402x^2 + 7.305x^3 + 2.889x^4 \\ -17.21 + 16x + 9.4x^2 - 7.305x^3 - 2.889x^4 \end{cases} \quad (19)$$

Fig. 5 showed the results of fitting the upper and lower body contours of the porpoise in the top view using a fourth-order Polynomial model. In the optimization process of the top view porpoise body contour equation system, the

procedure was identical to that used for the front view porpoise body contour equation system.

TABLE VI
Fitting results of upper body contour by different models

Number of terms or degree	Model	SSE	RMSE	R^2
1	Exponential	1170	7.136	0.145
	Fourier	288.9	3.560	0.789
	Gaussian	659.2	5.365	0.518
	Polynomial	113.1	7.014	0.174
	Power function	133.8	7.627	0.023
	Sine	938.8	6.402	0.314
2	Exponential	592.6	5.098	0.567
	Fourier	248.4	3.315	0.818
	Gaussian	376.4	4.081	0.725
	Polynomial	608.4	1.630	0.955
	Power function	105.0	6.373	0.233
	Sine	281.5	3.529	0.794
3	Fourier	226.7	3.181	0.834
	Gaussian	141.5	2.519	0.896
	Polynomial	609.9	1.635	0.955
	Sine	227.5	3.194	0.839
4	Fourier	166.9	2.742	0.878
	Gaussian	151.1	2.287	0.912
	Polynomial	130.0	1.032	0.992
	Sine	182.1	2.877	0.867
5	Fourier	159.6	2.696	0.883
	Gaussian	110.0	2.251	0.919
	Polynomial	400.5	1.331	0.970
	Sine	167.4	2.777	0.877
6	Fourier	134.4	2.483	0.901
	Gaussian	106.3	2.229	0.922
	Polynomial	492.6	1.479	0.964
	Sine	135.6	2.517	0.901
7	Fourier	122.3	2.380	0.910
	Gaussian	103.3	2.213	0.924
	Polynomial	228.3	3.196	0.962
	Sine	129.0	2.471	0.905
8	Fourier	128.4	2.405	0.920
	Gaussian	100.6	2.199	0.926
	Polynomial	200.6	1.391	0.968
	Sine	119.7	2.399	0.912

The top view porpoise body contour equation system $O_2(x)$ fitted by a Polynomial model was refined by removing the constant term and adding half the coefficient of the independent variable term. This could obtain the contour fitting equation system $C_2(x)$ of the top view porpoise that conformed to the NACA airfoil equation system form. The equation system was:

$$C_2(x) = \begin{cases} -(4.093e+12)x^{\frac{1}{2}} + (2.047e+12)x + 0.00103x^2 \\ \quad -(4.635e-0.5)x^3 + (1.548e-0.7)x^4 \\ (4.093e+12)x^{\frac{1}{2}} - (2.047e+12)x - 0.00103x^2 \\ \quad +(4.635e-0.5)x^3 - (1.548e-0.7)x^4 \end{cases} \quad (20)$$

Due to the symmetrical curve of the top view of the porpoise, a NACA four-digit symmetrical airfoil was used. Regression analysis was conducted on the equation $C_2(x)$ and the mathematical expressions of various NACA airfoils, with the result for SSE_2 between $C_2(x)$ and the equations of various NACA airfoil models was compared, as shown in Table VII. By analyzing Table VII, the NACA0015 airfoil demonstrated a better fit to the porpoise body contour and thus was selected as the contour equation for the porpoise in a stationary state. The parameters of the NACA0015 model correspond to the morphological characteristics of the porpoise, and their corresponding numerical values could be determined. As the airfoil of the NACA0015 model only had two parameters: chord length(c) and maximum thickness(t), and 15% of the chord length was the maximum thickness (t) of the airfoil(t=0.15c), it could be concluded that the contour equation for the top view of the porpoise was a four-digit symmetric NACA0015 airfoil profile, with its parameters being: c=226.2 and t=33.93.

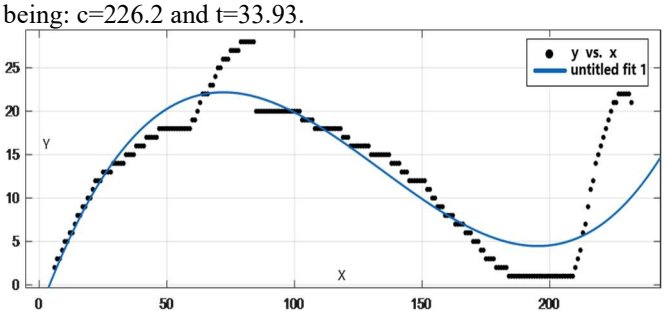

(a) The upper body contours

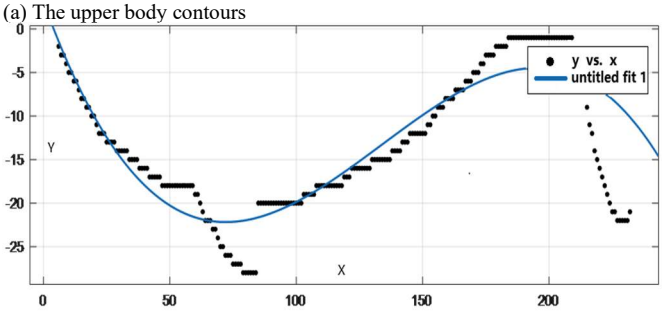

(b) The lower body contours

Fig. 5. Modeling schematic of the body contours in the top view of the porpoise

Furthermore, Fig. 6 was generated using a three-dimensional model, which illustrated the geometric characteristics of the porpoise from various perspectives, including the top view, front view, orthogonal view, and an angled top view. From an overall morphological perspective, the porpoise's contour presented a streamlined profile consistent with fluid dynamics optimization principles. This hydrodynamic design effectively reduced drag during aquatic locomotion, consequently enhancing swimming efficiency.

TBALE VII
The sum of the squared residuals from the regression of NACA airfoil equations and polynomial formulas

NACA airfoil model	SSE_2
0015	251.416129
0018	252.646526
0021	253.885579
0024	255.130725

Note: (SSE_2 represents the sum of squared residuals with the NACA equation and $C_2(x)$)

From the front view, the porpoise's contour was quite rounded at the front and gradually narrows towards the rear. This shape effectively reduced frontal resistance, allowing water to flow more smoothly around the body.

The orthogonal view revealed an approximately symmetrical elliptical cross-section, exhibiting structural parallels to the NACA four-digit airfoil profile (e.g., NACA0015). The geometric feature enhanced hydrodynamic stability and reduced energy loss associated with lateral oscillations.

From the top view, the porpoise's streamlined profile was further emphasized by its elongated, gradually tapering body, which reduced flow separation, minimized hydrodynamic wake turbulence, and optimized the thrust distribution from caudal fin movements.

An angled top view offered a more intuitive observation of the three-dimensional form, revealing that the curvatures of the upper and lower body were quite similar.

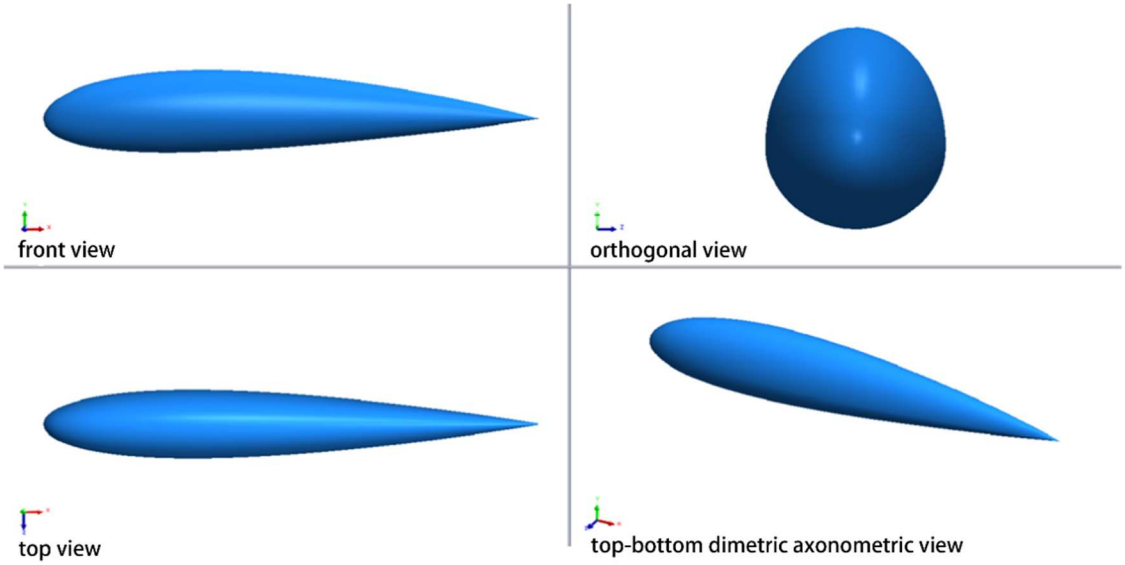

Fig.6. Schematic diagram of the three-dimensional modeling results of the porpoise body shape

This structural symmetry suggested that the porpoise maintained a stable swimming posture, thereby minimizing energy expenditure.

Overall, this figure demonstrated that the harbor porpoise's morphology aligns with the principles of hydrodynamic optimization. Its streamlined body shape is likely to enhance propulsion efficiency and reduce hydrodynamic drag during swimming.

IV. Discussion

A. Extraction of External Morphological Contours of Porpoises

Currently, computer vision had been widely applied as a key technological tool in bio morphological analysis and biomimetic design. He Qianhan et al. used computer vision technology to recognize and annotate the morphological features of the beak, thereby calculating its morphological parameters [18]. Tu Bing and colleagues demonstrated that fish body contours processed using computer vision could be used to calculate similarity values with established mathematical models of fish body contour curves. These similarity values could then be used to determine the species of target fish [20].

This study used PyCharm software to run the Canny algorithm to extract the optimal contour of the external morphology of the porpoise, and its feature points could be identified and obtained through the traversal algorithm. According to the contour map of the porpoise (Fig. 2), its outer contour could be divided into two layers: the inner contour layer and the outer contour layer. After performing edge detection on the image, there was no hierarchical relationship among the identified contours. These contour entities were independent of each other. Therefore, in the subsequent modeling process using the extracted contours of the porpoise and the curve mathematical model, it was only necessary to traverse the outer contours that had been extracted. Moreover, attention should be paid to changes in pixel values when acquiring parameters. Observations from Fig. 3, Fig. 4, and Fig. 5 revealed that the vertical pixel range of the initial contour image of the porpoise was from -30 to 30 (Fig. 3). After traversing and extracting the outer contours, the vertical range changed to between -25 and 25 (Fig. 4 and Fig. 5), while the horizontal pixel values remained unchanged.

The extraction of target contours and feature points using computer vision represented an intelligent, efficient, precise, and direct methodology. By leveraging this technological approach, porpoise contours could be modeled into standardized curve-based mathematical frameworks, thereby significantly advancing applied research on their external morphology.

B. Modeling the External Morphology of Porpoises

According to recent studies, bio morphological features extracted via computer vision technology had been applied in engineering design. Zhang Zhaohuang and Li Weiwei applied the extracted contour of the pectoral fins of humpback whales to the design of bionic blades with NACA634-021 airfoil sections. Studies had demonstrated that computer vision technology plays a key role in acquiring modeling data for engineering design [21]. Zhou Zupeng et al. used Polynomial models to fit the surface of the crocodile's upper jaw and combined reverse engineering technology with computer technology to accurately reconstruct the original model [28]. This study employed six mathematical models—Exponential, Fourier, Gaussian, Polynomial, Power function, and Sine function—to evaluate the extracted porpoise contours. Following a comprehensive analysis and comparative evaluation of porpoise contour modeling, the Polynomial model demonstrated the highest goodness-of-fit. Polynomial models relied on the least squares method, which exhibited reduced sensitivity to outliers and mitigates their influence during regression analysis to yield more robust regression coefficients. As a result, this model enabled a more accurate reconstruction of the porpoise body contour shape [27], [28], [29].

During the study, it was observed that the derived polynomial mathematical model resembles the NACA airfoil equation. After optimizing the Polynomial model into a NACA airfoil framework, the length of the porpoise body

could be calculated to be 226.2 pixels based on the extracted porpoise body contour feature points. The corresponding parameter in the NACA airfoil equation was chord length c=226.2. The remaining parameter values were determined based on the NACA wing profile designations NACA2408 and NACA0015. Therefore, integrating computer vision technology to extract porpoise feature points into modeling engineering practices not only established a robust mathematical foundation for subsequent bionic design research but also significantly enhanced the efficiency of bionic design processes.

V. Conclusion

This study introduces a novel framework for standardized modeling of porpoise's external morphology through computer vision techniques. Firstly, a computer vision-based preprocessing pipeline is implemented for porpoise images, enabling the extraction of the front view and top view body contours. Feature points are detected via a contour traversal algorithm. The extracted contours are then regressed using multiple mathematical curve models. Based on fitting accuracy and downstream engineering application requirements, two quartic polynomial curve equation systems are ultimately adopted to represent the front view and top view porpoise body contours, respectively. Through a comparative analysis of the derived quartic polynomial systems against NACA airfoil equations, NACA2408 and NACA0015 were identified as the optimal matches for the front and top view contours of the harbor porpoise, respectively. The experimental results demonstrate that the computer vision-based approach to porpoise external morphology modeling enables a more intuitive comparative analysis of shape characteristics. The obtained NACA airfoil equation system serves as a tool for porpoise morphological analysis and the subsequent design of bionic underwater vehicles compatible with porpoise body contours. It supports exploration of marine ecosystems and fishery resource diversity through technological advancements, while also offering new experimental insights for future work.

References

[1] Clara, Yang Fengli, "Sonar of rat dolphins," Global Science, no. 3, pp. 16-16, 2018.

[2] Leigh-Anne Dell, Nina Patzke, Muhammad A Spocter, Jerome M Siegel, Paul R Manger, "Organization of the sleep-related neural systems in the brain of the harbour porpoise (Phocoena phocoena)," The Journal of Comparative Neurology, vol. 524, no. 10, pp. 1999-2017, 2016.

[3] Masao Amano, Nobuyuki Miyazaki, "Geographic variation in external morphology of Dall's porpoise, Phocoenoides dalli," Aquatic Mammals, vol. 22, no. 3, pp. 167-174, 1996.

[4] Sun Yingying, "Adaptive evolution of genes related to whale body size," Nanjing: Nanjing Normal University, 2017.

[5] Dominique Stalder, Floris van Beest, Signe Sveegaard, Rune Dietz, Jonas Teilmann, Jacob Nabe-Nielsen, "Influence of environmental variability on harbour porpoise movement," Marine Ecology Progress Series, no. 648, pp. 207-219, 2020.

[6] Kong Xianghong, Huang Xiaoshuang, Liu Fan, et al, "Design and implementation of a fish symbiotic device based on bionic porpoise," Fisheries Modernization, vol. 48, no. 5, pp. 18-25, 2021.

[7] James R. Robbins, Lucy Babey, Clare B. Embling, "Citizen science in the marine environment: estimating common dolphin densities in the north-east Atlantic," PeerJ, PeerJ 8: e8335, 2020.

[8] Chen Li, "Rapid detection method for morphological parameters of large yellow croaker based on machine vision," Shanxi: Taiyuan University of Science and Technology, 2016.

[9] Yud-Ren Chen, Kuanglin Chao, Moon S Kim, "Machine vision technology for agricultural applications," Computers and Electronics in Agriculture, vol. 36, no. 2-3, pp. 173-191, 2002.

[10] Cheng Yao, Zhao Lei, Cheng Shan, et al, "Design of vehicle distance detection system based on machine vision," Journal of Metrology, vol. 41, no. 1, pp. 11-15, 2020.

[11] Maxime Vidal, Nathan Wolf, Beth Rosenberg, Bradley P Harris, Alexander Mathis, "Perspectives on individual animal identification from biology and computer vision," Integrative and Comparative Biology, vol. 61, no. 3, pp. 900-916, 2021.

[12] D.J. White, C. Svellingen, N.J.C. Strachan, "Automated measurement of species and length of fish by computer vision," Fisheries Research, vol. 80, no. 2-3, pp. 203-210, 2006.

[13] Yu Xinjie, Wu Xiongfei, Wang Jianping, Chen Li, Wang Lei, "Rapid detecting method for Pseudosciaena Crocea morphological parameters of based on the machine vision," Integrated Technology, vol. 3, no. 5, pp. 45-51, 2014.

[14] Huang Xiaoshuang, Liu Fan, Sun Wengjie, Kong Xianghong, Liu Bilin, Chen Xinjun, "Fluid morphology modeling and numerical simulation of biomimetic squid," Journal of Shanghai Ocean University, vol. 30, no. 5, pp. 884-892, 2021.

[15] Angelo Loy, Sara Busilacchi, Corrado Costa, Ludovic Ferlin, Stefano Cataudella," Comparing geometric morphometrics and outline fitting methods to monitor fish shape variability of Diplodus puntazzo (Teleostea: Sparidae)," Aquacultural Engineering, vol. 21, no. 4, pp. 271-283, 2000.

[16] This Journal News, "Sino-U.S.-Mexico cooperation on the protection of the Gulf of California totoaba and vaquita," China Fisheries, no.12, pp. 17, 2016.

[17] Shengxian Huang， Yu Hu， Ying Wang, "Research on aerodynamic performance of a novel dolphin head -shaped bionic airfoil," Energy, vol. 214, 118179, 2021.

[18] He Qianhan, Sun Wengjie, Liu Bilin, Kong Xianghong, Lin Longshan, "Morphological study on beak of cephalopods based on computer vision I: contour and feature point extraction," Oceanologia et Limnologia Sinica, vol. 51, no. 6, pp. 1493-1500, 2020.

[19] Zhang Zhiqiang, Niu Zhiyou, Zhao Siming, "Identification of freshwater fish species based on machine vision technology," Journal of Agricultural Engineering, vol. 27, no. 11, pp. 388-392, 2011.

[20] Tu Bing, Wang Jinping, Wang Sicheng, Zhou Xing, Dai Ping, "Research on identification of freshwater fish species based on fish back contour correlation coefficient," Computer Engineering and Applications, vol. 52, no. 16, pp. 162-166, 2016.

[21] Zhang Zhaohuang, Li Weiwei, "Aerodynamic characteristics of bionic of leading-edge of humpback whale flipper," Engineering Mechanics, vol. 37, no. S, pp. 376-379+386, 2020.

[22] Wang Xiaojun, Liu Xumin, Guan Yong, "Image edge detection algorithm based on improved Canny operator," Computer Engineering, vol. 38, no. 14, pp. 196-198+202, 2012.

[23] Zhao Jing, He Dongjian, "Studies on technique of computer recognition of fruit shape," Transactions of the Chinese Society of Agricultural Engineering, no. 2, pp. 165-167, 2001.

[24] Li Kuan, Zhang Peijun, Liu Mingzhong, Lin Mingli, Li Songhai, "Morphological measurements of a dead Indo-Pacific humpback dolphin (Sousa chinensis) at Sanya, Hainan Province, China," Acta Theriologica Sinica, vol. 38, no. 6, pp. 616-623, 2018.

[25] Zhu Qian, Li Xiang, Ma Mu, Jiang Bo, "Some measurements of the Spinner dolphin stennlla longirostris," Marine Sciences, no. 8, pp. 15-17, 2007.

[26] Zhang Shiqiang, "Approach on the fitting optimization index of curve regression," Chinese Journal of Health Statistics, vol. 19, no. 1, pp. 9-11, 2002.

[27] Shi Lixin, Nie Xintian, Ji Ming, "List curve fitting based on Matlab curve fitting toolbox," New Technology & New Process, no.7, pp. 39-42, 2007.

[28] Zhou Zupeng, Pei Yumeng, Josep Fortuny, Jordi Marcé Nogué, Jiang Kaiyun, Zhong Xuebo, "Surface fitting and deviation analysis of upper jaw morphology of crocodile," Journal of Shenyang University of Technology, vol. 43, no. 4, pp. 444-449, 2021.

[29] Ou li Guo, Liu Bilin, Fang zhou, "Identification of sagittal Otolith morphology and sulcus morphology based on elliptic Fourier transform," Marine Fisheries, vol. 41, no.4, pp. 385-396, 2019.